Limit

NASA TECHNICAL NOTE

NASA TN D-7491

NASA TN D-7491

FLUTTER OF ELASTICALLY SUPPORTED ORTHOTROPIC PANELS INCLUDING THE EFFECTS OF FLOW ANGLE

by James Wayne Sawyer

Langley Research Center

Hampton, Va. 23665

NATIONAL AERONAUTICS AND SPACE ADMINISTRATION • WASHINGTON, D. C. • MAY 1974

1. Report No.	2. Government Accession No.	3. Recipient's Catalog No.
NASA TN D-7491		

4. Title and Subtitle	5. Report Date
FLUTTER OF ELASTICALLY SUPPORTED ORTHOTROPIC PANELS INCLUDING THE EFFECTS OF FLOW ANGLE	May 1974
	6. Performing Organization Code
7. Author(s)	8. Performing Organization Report No.
James Wayne Sawyer	L-9312
	10. Work Unit No.
9. Performing Organization Name and Address	502-32-02-05
NASA Langley Research Center Hampton, Va. 23665	11. Contract or Grant No.
	13. Type of Report and Period Covered
12. Sponsoring Agency Name and Address	Technical Note
National Aeronautics and Space Administration Washington, D.C. 20546	14. Sponsoring Agency Code

15. Supplementary Notes

16. Abstract

A theoretical panel flutter analysis and computer program was developed which is capable of analyzing an orthotropic panel with in-plane loads, at various angles of cross flow and various edge-support conditions. The resulting modal analysis uses linear piston-theory aerodynamics and includes both aerodynamic and structural damping. Calculations made for typical panels with no in-plane forces show that large reductions in dynamic pressure for flutter are possible with only small changes in flow angle. The reduction in dynamic pressure with flow angle is greater for elastically supported panels than for simply supported panels. Aerodynamic damping has a significant stabilizing effect at all flow angles except zero, whereas structural damping has negligible effect.

17. Key Words (Suggested by Author(s))	18. Distribution Statement
Panel flutter Flow angle Orthotropic panels Elastic supports	Unclassified – Unlimited Star Category 32

19. Security Classif. (of this report)	20. Security Classif. (of this page)	21. No. of Pages	22. Price*
Unclassified	Unclassified	36	$3.25

*For sale by the National Technical Information Service, Springfield, Virginia 22151

FLUTTER OF ELASTICALLY SUPPORTED ORTHOTROPIC PANELS INCLUDING THE EFFECTS OF FLOW ANGLE

By James Wayne Sawyer
Langley Research Center

SUMMARY

A theoretical panel flutter analysis and computer program was developed which is capable of analyzing an orthotropic panel with in-plane loads, at various angles of cross flow and with two opposite edges mounted on flexible supports and the other two edges simply supported. The resulting modal analysis uses linear piston-theory aerodynamics and includes both aerodynamic and structural damping. Calculations were made for typical panels with no in-plane forces showing the effect on flutter of various deflectional edge-support conditions, flow angle, and aerodynamic and structural damping. The results show that large reductions in dynamic pressure for flutter are possible with only small changes in flow angle, and the reduction is greater for elastically supported panels than for simply supported panels. Aerodynamic damping has a significant stabilizing effect at all flow angles except zero, whereas structural damping has negligible effect.

INTRODUCTION

Interest in reentry and sustained high-speed flight has resulted in the need for a system to protect the vehicle's primary structure from high surface temperatures. Several types of thermal protection systems are being developed, including both metallic and nonmetallic heat shields. (See, for instance, refs. 1 to 4.) One type of thermal protection system of interest is shown in figure 1 and consists of a flexible thermal insulation blanket covered by a wavy metallic surface (corrugated or corrugation stiffened) which is attached to the primary structure by flexible supports. The supports must be flexible enough to allow thermal expansion without imposing large stresses but strong enough to transmit airloads to the primary structure. The wavy surface geometry required to accommodate thermal strain results in a panel with highly orthotropic stiffnesses which in service will experience flow over its surface at angles other than parallel to the corrugations. As a result of the flexible supports and flow angle, panel flutter becomes an important factor to consider in the design of such a panel. This dependence on flow angle and flexible supports has been shown experimentally in reference 5 in which orthotropic panels mounted

on flexible supports were shown to experience large reductions in critical flutter dynamic pressures for only small changes in flow angle.

Previous theoretical investigators have studied the influence of boundary conditions and flow angle on flutter of orthotropic panels separately. For example, references 2 and 6 to 9 have studied the effects of flexible supports on flutter for panels at flow angles of 0° and 90°, and references 10 to 13 have studied the effects of arbitrary flow angles on flutter for panels with classical (simply supported or clamped) boundary conditions. No theoretical panel flutter studies have been made, however, for panels mounted on flexible supports and at arbitrary flow angles.

The present investigation was undertaken to develop an analysis and computer program that is capable of analyzing an orthotropic panel at various flow angles and with two opposite edges mounted on flexible supports and the other two edges simply supported. The resulting modal analysis uses linear piston-theory aerodynamics and includes in-plane loads and both aerodynamic and structural damping. The aerodynamic theory treats the surface as a flat plate and does not take into account wavy surfaces such as shown in figure 1. The number of modes in each direction can be varied to insure that converged solutions are obtained. Results are presented for typical panels with no in-plane loads showing the effect on flutter of various edge-support conditions, flow angle, and aerodynamic and structural damping. Flutter mode shapes and frequencies are presented for a typical panel at various flow angles.

SYMBOLS

A	Fourier series coefficients (see eq. (6))
$\bar{A}$	quantity defined by equation (15a)
a	panel length (x-direction)
$\bar{B}$	frequency parameter defined by equation (15b)
b	panel width (y-direction)
C_{mn}	constant of integration
c	free-stream speed of sound
D_{mn}	constant of integration

D_x panel bending stiffness in x-direction

D_y panel bending stiffness in y-direction

D_{xy} panel twisting stiffness

$$D_1 = \frac{D_x}{1 - \mu_x\mu_y}$$

$$D_2 = \frac{D_y}{1 - \mu_x\mu_y}$$

$$D_{12} = D_{xy} + \mu_x D_2$$

g_a aerodynamic damping coefficient (see eqs. (13))

g_b bending structural damping coefficient

g_m membrane structural damping coefficient

K_d, K_r, K_t deflectional, rotational, and torsional spring constants, respectively, per unit length

$\bar{K}_d, \bar{K}_r, \bar{K}_t$ nondimensional deflectional, rotational, and torsional spring constants, respectively

M Mach number

m number of half-waves in streamwise direction

N_x, N_y uniform in-plane loads per unit length in x- and y-directions, respectively

n number of half-waves in cross-stream direction

q dynamic pressure of airstream

r, s integers

t time

w	lateral deflection of panel
w_{mn}	lateral deflection of panel describing shape of natural mode of vibration
X	function describing shape of natural mode of vibration in x-direction (see eqs. (16) and (17))
x,y	Cartesian coordinates of panel (see fig. 2)
$\bar{x},\bar{y}$	fixed coordinates based on stream direction (see fig. 2)
α	complex frequency coefficient
α_{mn}	complex natural frequency coefficient
β	compressibility factor
γ	panel mass per unit area
ϵ,δ	parameters associated with characteristic roots (see eqs. (18) and (19))
Λ	local cross-flow angle, deg
λ	dynamic-pressure parameter, $2qa^3/\beta D_1$
λ_{cr}	dynamic-pressure parameter at flutter
μ_x,μ_y	Poisson's ratio associated with curvature in y- and x-directions, respectively
ξ	nondimensional coordinate, x/a
η	nondimensional coordinate, y/b
ρ	free-stream air density
ψ	real part of complex-frequency coefficient
ω	imaginary part of complex-frequency coefficient

ω_r fundamental frequency of simply supported beam, $\left(\pi^2/a^2\right)\sqrt{D_1/\gamma}$, radians per second

Subscripts:

m,r number of half-waves in x-direction

n,s number of half-waves in y-direction

ANALYSIS

Flutter Equation

A flutter analysis is presented for a flat orthotropic panel with supersonic flow at Mach number, M, over one surface at arbitrary cross-flow angle, Λ. The panel and coordinate system are shown in figure 2. The panel edges at $x = \pm\frac{a}{2}$ are supported by deflectional, rotational, and torsional springs, and the other two edges (y = 0 and b) are simply supported. The panel is loaded by uniform in-plane loads, N_x and N_y, which are considered positive in compression. The aerodynamic loading is given by linear piston theory (which assumes a smooth exterior surface) and includes aerodynamic damping. The governing differential equation assuming linear small-deflection theory is (see ref. 10)

$$\left(1 + ig_b\right)\left(D_1 \frac{\partial^4 w}{\partial x^4} + 2D_{12} \frac{\partial^4 w}{\partial x^2 \partial y^2} + D_2 \frac{\partial^4 w}{\partial y^4}\right) + \left(1 + ig_m\right)\left(N_x \frac{\partial^2 w}{\partial x^2} + N_y \frac{\partial^2 w}{\partial y^2}\right) + \gamma \frac{\partial^2 w}{\partial t^2} + \rho c \frac{\partial w}{\partial t} + \frac{2q}{\beta} \frac{\partial w}{\partial \bar{x}} = 0 \tag{1}$$

where

$$D_1 = \frac{D_x}{1 - \mu_x \mu_y}$$

$$D_2 = \frac{D_y}{1 - \mu_x \mu_y}$$

$$D_{12} = D_{xy} + \mu_x D_2$$

g_b and g_m are bending and membrane structural damping coefficients (see ref. 14), and $\rho c \frac{\partial w}{\partial t}$ is the aerodynamic damping term. After transforming the aerodynamic loading terms to panel coordinates (see fig. 2) and nondimensionalizing, equation (1) becomes

$$\left(1 + ig_b\right)\left[\frac{\partial^4 w}{\partial \xi^4} + \frac{2D_{12}}{D_1}\left(\frac{a}{b}\right)^2 \frac{\partial^4 w}{\partial \xi^2 \partial \eta^2} + \left(\frac{a}{b}\right)^4 \left(\frac{D_2}{D_1}\right)\left(\frac{\partial^4 w}{\partial \eta^4}\right)\right]$$

$$+ \left(1 + ig_m\right)\left[\frac{N_x a^2}{D_1}\left(\frac{\partial^2 w}{\partial \xi^2}\right) + \frac{N_y a^4}{D_1 b^2}\left(\frac{\partial^2 w}{\partial \eta^2}\right)\right] + \frac{\gamma a^4}{D_1}\left(\frac{\partial^2 w}{\partial t^2}\right)$$

$$+ \frac{\rho c a^4}{D_1}\left(\frac{\partial w}{\partial t}\right) + \frac{2qa^3}{\beta D_1}\left[(\cos \Lambda)\frac{\partial w}{\partial \xi} + \frac{a}{b}(\sin \Lambda)\frac{\partial w}{\partial \eta}\right] = 0 \tag{2}$$

The boundary conditions at the simply supported edges are

$$w(x,0,t) = w(x,1,t) = \frac{\partial^2 w}{\partial \eta^2}(x,0,t) = \frac{\partial^2 w}{\partial \eta^2}(x,1,t) = 0 \tag{3}$$

At the spring-supported edges, the boundary conditions obtained from reference 15 are

$$\left[\frac{\partial^2 w}{\partial \xi^2} + \mu_y\left(\frac{a}{b}\right)^2\left(\frac{\partial^2 w}{\partial \eta^2}\right) \pm \bar{K}_r\left(\frac{\partial w}{\partial \xi}\right)\right]_{\xi = \pm \frac{1}{2}} = 0 \tag{4}$$

$$\left[\bar{K}_d w \mp \bar{K}_t\left(\frac{a}{b}\right)^2\left(\frac{\partial^2 w}{\partial \eta^2}\right) - 2\left(\frac{a}{b}\right)^2\left(\frac{2D_{xy} + \mu_x D_2}{D_1}\right)\left(\frac{\partial^3 w}{\partial \eta^2 \partial \xi}\right) - \frac{\partial^3 w}{\partial \xi^3}\right.$$

$$\left. - \frac{N_x}{D_1}\left(a^2\right)\left(\frac{\partial w}{\partial \xi}\right)\right]_{\xi = \pm \frac{1}{2}} = 0 \tag{5}$$

where

$$\bar{K}_d = \frac{K_d a^3}{D_1}$$

$$\bar{K}_r = \frac{K_r a}{D_1}$$

$$\bar{K}_t = \frac{K_t a}{D_1}$$

and K_d, K_r, and K_t are the respective deflectional, rotational, and torsional spring constants per unit length.

Flutter Solution

Assume the solution of equation (2) to be in the form

$$w = \sum_{m=1}^{\infty} \sum_{n=1}^{\infty} A_{mn} w_{mn} e^{\alpha t} \tag{6}$$

where $\alpha = \psi + i\omega$. The natural mode shapes, w_{mn}, satisfy the boundary conditions, equations (3), (4), and (5), and the following natural vibration equation obtained by setting the dynamic terms in equation (2) equal to zero:

$$\begin{aligned}
&\left(1 + ig_b\right)\left[\frac{\partial^4 w_{mn}}{\partial \xi^4} + 2\left(\frac{a}{b}\right)^2\left(\frac{D_{12}}{D_1}\right)\left(\frac{\partial^4 w_{mn}}{\partial \xi^2 \partial \eta^2}\right) + \left(\frac{a}{b}\right)^4\left(\frac{D_2}{D_1}\right)\left(\frac{\partial^4 w_{mn}}{\partial \eta^4}\right)\right] \\
&+ \left(1 + ig_m\right)\left[\frac{N_x a^2}{D_1}\left(\frac{\partial^2 w_{mn}}{\partial \xi^2}\right) + \frac{N_y a^4}{b^2 D_1}\left(\frac{\partial^2 w_{mn}}{\partial \eta^2}\right)\right] \\
&+ \frac{\gamma a^4}{D_1}\alpha_{mn}^2 w_{mn} + \frac{\rho c a^4}{D_1}\alpha_{mn} w_{mn} = 0
\end{aligned} \tag{7}$$

The complex frequency coefficient, α_{mn}, is the damped natural frequency coefficient of the mnth mode.

Substituting the expression for w given by equation (6) into equation (2) and making use of equation (7) results in the following:

$$\begin{aligned}
&\sum_{m=1}^{\infty} \sum_{n=1}^{\infty} \left\{ \frac{\gamma a^4}{D_1}\left(\alpha_{mn}^2 - \alpha^2\right) w_{mn} + \frac{\rho c a^4}{D_1}\left(\alpha_{mn} - \alpha\right) w_{mn} \right. \\
&\left. + \frac{2qa^3}{\beta D_1}\left[(\cos \Lambda)\frac{\partial w_{mn}}{\partial \xi} + \frac{a}{b}(\sin \Lambda)\left(\frac{\partial w_{mn}}{\partial \eta}\right)\right]\right\} A_{mn} = 0
\end{aligned} \tag{8}$$

If w_{mn} is taken in the form

$$w_{mn} = X_{mn}(\xi)(\sin n\pi\eta) \tag{9}$$

the term $\sin n\pi\eta$ satisfies the boundary conditions, equation (3), directly. A Galerkin type solution is then obtained by substituting the expression for w_{mn} given by equation (9)

into equation (8), multiplying through by $X_{rs} \sin s\pi\eta$, and integrating over the total area. Performing the integration and rearranging the terms results in the following set of simultaneous equations:

$$A_{mn}\left[\frac{1}{\omega_r{}^2}\left(\alpha_{mn}^2 - \alpha^2\right) + \frac{g_a}{\omega_r}\left(\alpha_{mn} - \alpha\right)\right] + \frac{\lambda(\cos\Lambda)}{\pi^4}\sum_{r=1}^{\infty} A_{rn}\frac{Q_{mrns}}{P_{mrns}}$$

$$+ \frac{2\lambda a}{\pi^4 b}\sum_{s=1}^{\infty}\frac{A_{ms}ns\left(1 - (-1)^{s+n}\right)}{\pi^4 b\left(s^2 - n^2\right)}\sin\Lambda = 0 \qquad (n \neq s) \qquad (10)$$

where

$$Q_{mrns} = \int_{-1/2}^{1/2}\frac{\partial X_{mn}}{\partial x}X_{rs}\,dx \qquad (11)$$

$$P_{mrns} = \int_{-1/2}^{1/2} X_{mn}X_{rs}\,dx \qquad (12)$$

and

$$\left.\begin{aligned}\omega_r{}^2 &= \frac{\pi^4 D_1}{\gamma a^4}\\ g_a &= \frac{\rho c}{\gamma\omega_r}\\ \lambda &= \frac{2qa^3}{\beta D_1}\end{aligned}\right\} \qquad (13)$$

For a nontrivial solution to equation (10), the determinant of the coefficients of A_{mn} must equal zero. A standard eigenvalue routine for a square complex matrix was used to calculate the eigenvalues of equation (10) which render the determinant equal to zero. The complex frequency coefficients, α, are the eigenvalues. Flutter is considered to occur for that value of the dynamic-pressure parameter, λ, for which one of the imaginary frequencies changes sign (see ref. 14).

Natural Modes and Frequencies

The natural (no-flow) mode shapes, X_{mn}, and frequency coefficients, α_{mn}, are needed to determine the coefficients in equation (10). These are obtained from the

differential equation (7) and boundary conditions, equations (4) and (5). Substituting equation (9) into equation (7) results in the following differential equation, in X_{mn}:

$$X_{mn}^{IV} + \bar{A}\pi^2 X_{mn}'' - \bar{B}\pi^4 X_{mn} = 0 \tag{14}$$

where

$$\bar{A} = \left(\frac{1 + ig_m}{1 + ig_b}\right)\frac{N_x a^4}{D_1 \pi^2} - 2\left(\frac{a}{b}\right)^2 \frac{D_{12}}{D_1} n^2 \tag{15a}$$

$$\bar{B} = \left(\frac{1 + ig_m}{1 + ig_b}\right)\frac{N_y a^4}{D_1 b^2 \pi^2} - \left(\frac{an}{b}\right)^4 \frac{D_2}{D_1} - \frac{\gamma a^4 \alpha^2}{D_1 \pi^4 (1 + ig_b)} - \frac{\rho c a^2 \alpha}{D_1 \pi^4 (1 + ig_b)} \tag{15b}$$

Appropriate mode shapes which satisfy the boundary conditions, equations (4) and (5), are given as follows (see ref. 7):

For even modes

$$X_{mn} = C_{mn} \cosh \epsilon_{mn}\xi + D_{mn} \cos \delta_{mn}\xi \tag{16}$$

For odd modes

$$X_{mn} = C_{mn} \sinh \epsilon_{mn}\xi + D_{mn} \sin \delta_{mn}\xi \tag{17}$$

The relationship between ϵ_{mn} and δ_{mn} and the coefficients of equation (14) are obtained upon substitution of equation (16) or equation (17) into equation (14):

$$\epsilon_{mn} = \pi\left(-\frac{\bar{A}}{2} \pm \sqrt{\frac{\bar{A}^2}{4} + \bar{B}}\right)^{1/2} \tag{18}$$

and

$$\delta_{mn} = \pi\left(\frac{\bar{A}}{2} \pm \sqrt{\frac{\bar{A}^2}{4} + \bar{B}}\right)^{1/2} \tag{19}$$

In order to satisfy the boundary conditions, the expressions for X_{mn} given by equations (16) and (17) are substituted into equation (9) which is then substituted into equations (4) and (5). Solution to the resulting two simultaneous equations provides a transcendental equation in ϵ_{mn} and δ_{mn}.

Method of Computation

In order to obtain the aerodynamic coefficients of the flutter determinant (eq. (10)), mode shapes and frequencies are required. These are obtained for a given value of $\overline{A}$ by choosing $\overline{B}$ and solving for ϵ_{mn} and δ_{mn} in equations (18) and (19). These values are then substituted into the transcendental equation. If the transcendental equation is not satisfied, $\overline{B}$ is varied and the process is repeated. With the final values of ϵ_{mn} and δ_{mn}, the mode shapes, X_{mn}, are defined within an arbitrary constant and the frequency coefficients, α_{mn}, are obtained from equation (15b). Since the coefficients as defined by equations (15) are complex, the resulting frequencies are complex quantities.

When flow angle is not a variable, general flutter calculations can be made that cover a wide range of panels. Two geometry-stiffness parameters that are usually specified in the literature (see ref. 6) and supply all the information needed to make general calculations for zero flow angle are

$$\overline{A}_x = -2\left(\frac{a}{b}\right)^2 \frac{D_{12}}{D_1}$$

$$C = \frac{D_{12}}{\sqrt{D_1 D_2}}$$

These parameters are sufficiently general that one solution is applicable to panels with various length-width and stiffness ratios. With the inclusion of flow angle, however, equation (10) shows that the panel length-width ratio, a/b, must also be specified. By specifying a/b, the parameters $\overline{A}_x$ and C become functions only of the ratios of flexural stiffness properties, D_{12}/D_1 and D_{12}/D_2. Thus, flutter calculations must be made for the specific panel of interest. Flutter results are presented in the next section for panels with a wide range of stiffness parameters.

RESULTS AND DISCUSSION

Range of Parameters

Calculations were made for a wide range of flow angularity, boundary conditions, and panel characteristics. Flow angle was varied between 0° and 90°, and calculations

were made for deflectional spring stiffness, $\overline{K}_d$, of 10, 100, 500, and ∞. In order to keep the variables to a reasonable number, however, in-plane loads, N_x and N_y, and spring supports, $\overline{K}_r$ and $\overline{K}_t$, were set equal to zero. Aerodynamic and structural damping coefficients, g_a, g_b, and g_m, were set equal to zero for all panels except for one representative panel, which was used to study the effects of damping on flutter. Calculations were made for D_{12}/D_1 of 0.05, 0.25, and 0.50; D_{12}/D_2 of 2, 20, 50, and 500; and $(a/b)^2$ of 1.0 and 10. This range of parameters was chosen because they include most orthotropic panels that have been investigated either experimentally or theoretically in the literature (see, for instance, ref. 16) and most panels that are of current interest.

Convergence

In normal-mode flutter analyses, one of the questions that naturally arises is how many modal terms are required to obtain a converged solution. Previous studies have shown that, for flow parallel to a panel edge (zero flow angle), one modal term normal to that edge is sufficient in flutter analyses, and the number of modal terms required parallel to the edge depends on the degree of orthotrophy (see, for example, ref. 7). When the flow angle is not zero, however, several modal terms may be required in both directions, but the number is dependent on panel orientation and boundary conditions. Using more modal terms than are necessary results in a considerable waste in computer run time and storage and may make the solution prohibitively costly.

Convergence data are given in figures 3(a), 3(b), and 3(c) where $\lambda^{1/3}$ is shown as a function of the number of modal terms for a typical orthotropic panel with various deflectional spring edge support conditions and at flow angles of 0°, 90°, and 10°, respectively. Calculations are made for $D_{12}/D_1 = 0.5$, $D_{12}/D_2 = 500$, and $(a/b)^2 = 1.0$. For the extreme orientations ($\Lambda = 0^\circ$ and 90°), calculations indicate only one modal term is required in the direction perpendicular to the flow to obtain converged solutions regardless of boundary conditions. For $\Lambda = 0^\circ$ (see fig. 3(a), direction of maximum flexural stiffness alined with flow), converged flutter values are obtained for only four terms in the D_1 direction for all values of $\overline{K}_d$ for which calculations were made. For $\overline{K}_d = \infty$, the $\lambda^{1/3}$ values converge to the exact value obtained from reference 17. The converged $\lambda^{1/3}$ value for $\overline{K}_d = 10$ is slightly higher than the exact value shown for free edge conditions $\left(\overline{K}_d = 0\right)$ (see ref. 7). For $\Lambda = 90^\circ$ (see fig. 3(b)), the situation is quite different, as converged results are seen to be strongly dependent on the boundary conditions. Converged flutter values are obtained with four terms in the D_2 direction for $\overline{K}_d = 10$, with eight terms in the D_2 direction for $\overline{K}_d = 100$, and with 20 terms in the D_2 direction for $\overline{K}_d = 500$. For $\overline{K}_d = \infty$ (simply supported edge), the flutter solution is not converged when even 60 terms are used; $\lambda^{1/3}$ is considerably below the exact value and, further, convergence is extremely slow. Thus, for orthotropic panels with simply supported edges

with flow normal to the direction of maximum flexural stiffness, a large number of modal terms are needed to obtain converged solutions. Similar trends have also been found to be true for panels with clamped edges (see ref. 13). As $\overline{K}_d$ decreases, however, the number of terms required for convergence decreases rapidly. When using only the first two terms in the D_2 direction (n = 1,2) for $\overline{K}_d = 100$ and 500 (see fig. 3(b)), $\lambda^{1/3}$ is seen to be considerably higher than the converged values. For these values of $\overline{K}_d$, higher modes coalesce for the lowest value of $\lambda^{1/3}$, and the absence of these modes in the two-term solution results in erroneous values.

Convergence results for flow at $\Lambda = 10^\circ$ are shown in figure 3(c) where $\lambda^{1/3}$ is plotted against the number of modal terms in the D_2 direction. Flutter points are shown for D_1 modal terms from 1 to 5. For $\Lambda = 10^\circ$, one term in the D_1 direction still gives converged solutions for $\overline{K}_d = 10$, 100, and 500 and for 4, 8, and 16 terms in the D_2 direction, respectively. For $\overline{K}_d = \infty$ (simply supported), however, one term in the D_1 direction results in a diverging solution which becomes progressively worse as more terms in the D_2 direction are included in the calculations. When three terms are used in the D_1 direction, only four terms are required in the D_2 direction to give converged flutter values for $\overline{K}_d = \infty$.

The variation in the modal terms required for convergence is shown in figure 4 where $\lambda^{1/3}$ is plotted as a function of flow angle for $D_{12}/D_1 = 0.5$, $D_{12}/D_2 = 500$, and $(a/b)^2 = 1.0$. The curves are the flutter boundaries for the values of $\overline{K}_d$ shown. The numbers in parentheses indicate the number of terms in the D_1 and D_2 directions required to obtain convergence within ±2 percent. The $\overline{K}_d = \infty$ curve is not shown for $\Lambda > 10^\circ$ owing to the large amount of computer time required for convergence. The data show that, even for small flow angles, considerably more D_2 terms are required for convergence than D_1 terms. For $\Lambda \geq 30^\circ$ only one term in the D_1 direction is required for all $\overline{K}_d$ values shown, and the number of terms required in the D_2 direction for $\Lambda = 30^\circ$ is adequate for all higher values of Λ.

Flutter Frequencies and Mode Shapes

Further insight into the modal terms required for convergence can be gained through examination of the influence of flow angle on frequencies and mode shapes. Panel frequencies for $D_{12}/D_1 = 0.5$, $D_{12}/D_2 = 500$, and $(a/b)^2 = 1.0$ with $\overline{K}_d = 100$ are shown in figure 5 as a function of λ for flow angles of 0°, 2°, 15°, and 90°. For $\Lambda = 0^\circ$ (fig. 5(a)), increasing λ results in the coalescence of the frequencies of modes m = 1 and 2 and n = 1 at $\lambda_{cr} \cong 118$. Further increases in λ result in a pair of frequencies becoming complex conjugates as shown by the dashed curve. Although the (1,1) and (1,2) frequencies are identical at $\lambda \cong 75$, panel instability does not occur. For $\Lambda = 2^\circ$ (fig. 5(b)), however, coalescence of the (1,1) and (1,2) modes does occur at

$\lambda_{cr} \cong 70$ and remains unstable for further increases in λ. In reference 10, where two terms were used in each direction, a stable region was found at values of λ greater than the initial instability value. Such a stable region clearly does not exist if a sufficient number of modes are used in the analysis. These data also suggest that, for small increases in Λ from zero, large reductions in critical dynamic pressure occur. This behavior must be taken into account in the design of wavy (highly orthotropic) surface panels since some cross flow will be experienced in actual flight.

For $\Lambda = 15^{\circ}$ (fig. 5(c)), the (1,3) and (1,4) modes coalesce at a λ_{cr} value of approximately 17, which represents a large drop from that obtained at $\Lambda = 2^{\circ}$. For $\Lambda = 90^{\circ}$ (fig. 5(d)), the (1,3) and (1,4) modes still coalesce but for values of $\lambda_{cr} \cong 5$.

The flutter mode shapes for $D_{12}/D_1 = 0.5$, $D_{12}/D_2 = 500$, $(a/b)^2 = 1$, and $\overline{K}_d = 100$ are shown in figure 6 for flow angles of 0°, 2°, 15°, and 90°. For $\Lambda = 0^{\circ}$ (fig. 6(a)), the mode shape has two half-waves in the direction of maximum panel flexural stiffness and one half-wave in the direction of minimum panel flexural stiffness. The maximum deflection occurs on the downstream portion of the panel. At $\Lambda = 2^{\circ}$ (fig. 6(b)), the flutter mode shape is considerably different from that at $\Lambda = 0^{\circ}$, with the maximum deflection shifting in the direction of minimum flexural stiffness. At a flow angle of 15° (fig. 6(c)) the flutter mode shape is complicated but basically is composed of three half-waves in the direction of minimum flexural stiffness and one half-wave in the opposite direction. Further increases in Λ have little additional effect on this mode shape (see fig. 6(d) for $\Lambda = 90^{\circ}$).

Parametric Studies

Effects of flow angle.- The effects of flow angle on flutter are shown in figure 7 where flutter boundaries are presented as a function of flow angle for $D_{12}/D_1 = 0.05$ and $(a/b)^2 = 10$. Boundaries are shown for $\overline{K}_d = 10$ (fig. 7(a)), $\overline{K}_d = 100$ (fig. 7(b)), and $\overline{K}_d = \infty$ (fig. 7(c)). The curves of each figure are for values of D_{12}/D_2 of 2, 20, 50, and 500. The actual calculations are indicated by the symbols on the curves. For $\overline{K}_d = 10$ (fig. 7(a)) and $D_{12}/D_2 = 500$, an order-of-magnitude reduction in the flutter dynamic pressure occurs over the first 10°, with less severe reductions thereafter. For smaller values of D_{12}/D_2 (corresponding to increases in D_2), the reduction in flutter dynamic pressure with flow angle is less and is spread out over a wider flow-angle range. For $D_{12}/D_2 = 2$, even an increase in the flutter dynamic pressure is obtained with increasing flow angles over most of the flow-angle range. This latter behavior is similar to that expected for an isotropic panel with a similar a/b ratio. Two points are shown at $\Lambda = 0^{\circ}$ for $D_{12}/D_2 = 500$ and are connected by a dashed line. The upper point is the critical flutter value at $\Lambda = 0^{\circ}$ and is the same for all values of D_{12}/D_2. The lower point is the value of λ where the two lowest frequencies cross

(see fig. (5)). Increasing the flow angle from zero results in the critical flutter λ dropping from the higher value at $\Lambda = 0^{\circ}$ to the lower curve for a very small Λ (for example, $\Lambda \leq 1^{\circ}$). Thus, for all practical purposes, the lower values should be used, even for $\Lambda = 0^{\circ}$.

Increasing the deflection spring stiffness, $\overline{K}_d$, to 100 (fig. 7(b)) and ∞ (fig. 7(c)) results in flutter boundaries similar to those obtained for $\overline{K}_d = 10$ but higher throughout the flow-angle range.

Flutter boundaries for $D_{12}/D_1 = 0.25$ and 0.5 are shown in figures 8 and 9, respectively, and have trends similar to those discussed previously for $D_{12}/D_1 = 0.05$. Panels with large D_{12}/D_1 values are more stable, however, as indicated by higher values of λ throughout the flow-angle range. For $D_{12}/D_1 = 0.25$ (fig. 8) and $\Lambda = 0^{\circ}$, note that λ_{cr} is lower for $\overline{K}_d = 100$ than for $\overline{K}_d = 10$. This unusual trend has been shown previously by an exact analysis in reference 7 and is attributed to a change in the flutter mode. With $\overline{K}_d = 10$ the lower vibration modes approach those of rigid-body translation and rotation and the panel becomes more resistant to flutter. At $D_{12}/D_1 = 0.5$ (fig. 9), this phenomenon does not occur.

Effects of flexural stiffness.- The data presented in figures 7 to 9 are replotted in figure 10 as a function of D_{12}/D_1 for flow angles of 0°, 5°, 10°, and 20°. Flutter values nondimensionalized by $\lambda_{cr_{(\overline{K}_d=\infty)}}$ (the value of λ for a simply supported panel at the flow angle in question) are shown for $(a/b)^2 = 10$, $\overline{K}_d = 100$, and D_{12}/D_2 of 2, 20, 50, and 500. In figure 10(a), the boundaries for $\Lambda = 0^{\circ}$ are independent of values of D_{12}/D_2 and are, therefore, functions only of $\overline{K}_d$. Increasing values of stiffness ratio, D_{12}/D_1, result in flutter boundaries approaching those for the simply supported panel $\left(\overline{K}_d = \infty\right)$. The flutter boundary is also shown for $\overline{K}_d = 10$ because of its peculiar trend. The unusual behavior for $\overline{K}_d = 10$ is due to the phenomenon that was noted previously in the discussion of figure 8 for $D_{12}/D_1 = 0.25$. Flutter values are obtained for $\overline{K}_d = 10$ that are even higher than for simply supported panels for the range of D_{12}/D_1 from 0.1 to 0.2. This behavior is consistent with results obtained from an exact analysis presented in reference 7.

Flutter boundaries for $\Lambda > 0^{\circ}$ are seen to be dependent on both D_{12}/D_1 and D_{12}/D_2. For small values of D_{12}/D_1 $\left(\text{for example, } D_{12}/D_1 = 0.05\right)$, increases in D_2 $\left(D_{12}/D_2 \text{ decreases}\right)$ have little effect on λ; however, for large values of D_{12}/D_1 $\left(\text{for example, } D_{12}/D_1 = 0.5\right)$ increases in D_2 have a large effect on λ. Note also that the influence of D_{12}/D_1 is strongly dependent on the flow angle; for example, with $\Lambda \geq 10^{\circ}$ and $D_{12}/D_2 > 50$, changes in D_1 have negligible influence on flutter. Thus, the curves tend to identify the range of influence of stiffnesses D_1 and D_2 and flow angle on panel flutter.

Effects of length-width ratio.- Flutter boundaries for $D_{12}/D_1 = 0.5$ and $(a/b)^2 = 1.0$ are presented in figure 11. The effects of panel length-width ratio on the flutter boundaries may be seen by comparing the boundaries given in figure 11 with those presented in figure 9. Reducing the panel length-width ratio has a large destabilizing effect as indicated by considerably lower values of λ throughout the flow-angle and $\overline{K}_d$ range. The destabilizing effect is more pronounced for elastically supported panels than for simply supported panels.

Effects of Aerodynamic and Structural Damping

The effects of aerodynamic and structural damping on the flutter of unstressed orthotropic panels are shown in figure 12. Calculations are made for $D_{12}/D_1 = 0.5$, $D_{12}/D_2 = 500$, $(a/b)^2 = 1.0$, $\overline{K}_d = 100$, and for values of $g_a = 0.2$ and $g_b = 0.05$. The membrane structural damping coefficient, g_m, is not considered since it has an effect only if there are in-plane forces acting on the panel. As can be seen, aerodynamic damping has a significant stabilizing effect at all flow angles except zero, whereas structural damping has negligible effect.

CONCLUDING REMARKS

A theoretical panel flutter analysis and computer program was developed which is capable of analyzing an orthotropic panel with in-plane loads, at various angles of cross flow, and with two opposite edges mounted on flexible supports and the other two edges simply supported. The resulting modal analysis uses linear piston-theory aerodynamics and includes both aerodynamic and structural damping. The number of modal terms used in each direction to analyze the panel can be varied to insure that converged solutions are obtained.

The inclusion of cross-flow angle as a variable in a panel flutter analysis requires that the panel geometry/stiffness properties be defined. Thus, flutter calculations must be made for each specific panel. Calculations made for typical unstressed orthotropic panels with deflectional spring supports indicate that fewer modal terms are required for converged solutions for elastically supported panels than for simply supported panels.

The calculations further show that an order-of-magnitude reduction in flutter dynamic pressure is possible with only small changes in flow angle. Also, the effects of flow angle are more pronounced for elastically supported panels than for simply supported panels. In addition, the results indicate that the influence of flexural stiffness, D_1, on flutter of elastically supported panels diminishes with small increases in flow angle from zero and that the range of influence of flexural stiffness can be identified as a function of flow angle.

REFERENCES

1. Anderson, Roger A.; Brooks, William A., Jr.; Leonard, Robert W.; and Maltz, Joseph: Structures – A Technology Overview. Astronaut. & Aeronaut., vol. 9, no. 2, Feb. 1971, pp. 38-47.

2. Bohon, Herman L.; and Shore, Charles P.: Application of Recent Panel Flutter Research to the Space Shuttle. Pt. II – Influence of Edge Clips and Flow Angularity. NASA Space Shuttle Technology Conference, Vol. III – Dynamics and Aeroelasticity, NASA TM X-2274, 1971, pp. 247-264.

3. Brewer, R. A.; Saydah, A. R.; Nestler, D. E.; and Florence, D. E.: Thermal Performance Evaluation of RSI Panel Gaps for Space Shuttle Orbiter. J. Spacecraft, vol. 10, no. 1, Jan. 1971, pp. 23-28.

4. Stein, Bland A.; Bohon, Herman L.; and Rummler, Donald R.: An Assessment of Radiative Metallic Thermal Protection Systems for Space Shuttle. NASA Space Shuttle Technology Conference – Dynamics and Aeroelasticity; Structures and Materials, NASA TM X-2570, 1972, pp. 267-302.

5. Shyprykevich, P.; and Sawyer, J. W.: Orthotropic Panel Flutter at Arbitrary Yaw Angles – Experiment and Correlation With Theory. AIAA Paper No. 73-192, Jan. 1973.

6. Bohon, Herman L.; Anderson, Melvin S.; and Heard, Walter L., Jr.: Flutter Design of Stiffened-Skin Panels for Hypersonic Aircraft. NASA TN D-5555, 1969.

7. Bohon, Herman L.; and Anderson, Melvin S.: Role of Boundary Conditions on Flutter of Orthotropic Panels. AIAA J., vol. 4, no. 7, July 1966, pp. 1241-1248.

8. Heard, Walter L., Jr.; and Bohon, Herman L.: Natural Vibration and Flutter of Elastically Supported Corrugation-Stiffened Panels – Experiment and Theory. NASA TN D-5986, 1970.

9. Erickson, Larry L.: Supersonic Flutter of Flat Rectangular Orthotropic Panels Elastically Restrained Against Edge Rotation. NASA TN D-3500, 1966.

10. Bohon, Herman L.: Flutter of Flat Rectangular Orthotropic Panels With Biaxial Loading and Arbitrary Flow Direction. NASA TN D-1949, 1963.

11. Kordes, Eldon E.; and Noll, Richard B.: Theoretical Flutter Analysis of Flat Rectangular Panels in Uniform Coplanar Flow With Arbitrary Direction. NASA TN D-1156, 1962.

12. Eisley, J. G.; and Luessen, G.: The Flutter of Thin Plates Under Combined Shear and Normal Edge Forces Including the Effects of Varying Sweepback. Paper No. 62-90, Inst. Aerospace Sci., June 1962.

13. Gaspers, Peter A., Jr.; Redd, Bass: A Theoretical Analysis of the Flutter of Orthotropic Panels Exposed to a High Supersonic Stream of Arbitrary Direction. NASA TN D-3551, 1966.

14. Shore, Charles P.: Effects of Structural Damping on Flutter of Stressed Panels. NASA TN D-4990, 1969.

15. Libove, Charles; and Batdorf, S. B.: A General Small-Deflection Theory for Flat Sandwich Plates. NACA Rep. 899, 1948. (Supersedes NACA TN 1526.)

16. Bohon, Herman L.: Flutter of Corrugation-Stiffened Panels at Mach 3 and Comparison With Theory. NASA TN D-4321, 1968.

17. Bohon, Herman L.; and Dixon, Sidney C.: Some Recent Developments in Flutter of Flat Panels. J. Aircraft, vol. 1, no. 5, Sept.-Oct. 1964, pp. 280-288.

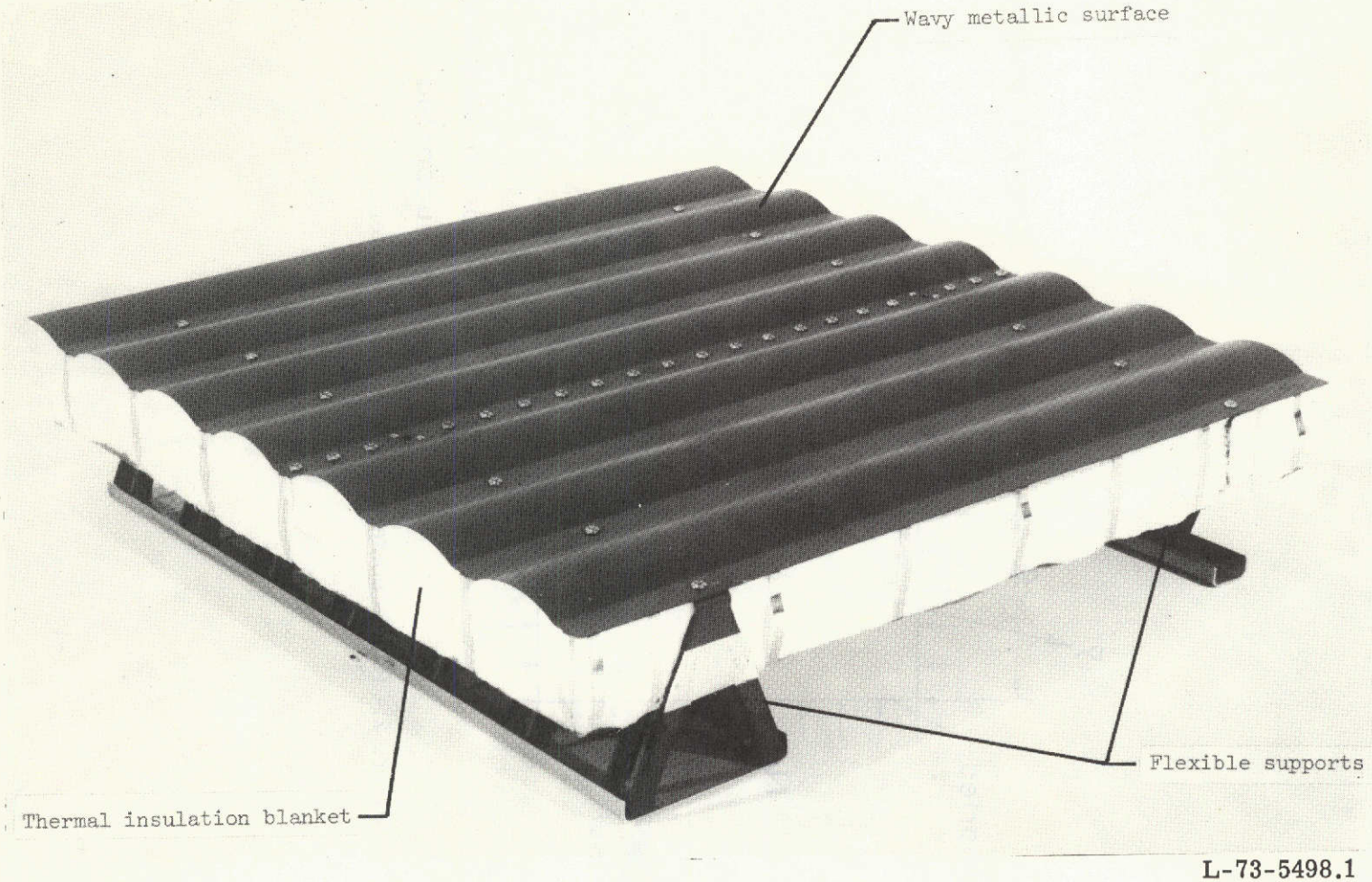

Figure 1.- Typical metallic thermal protection system.

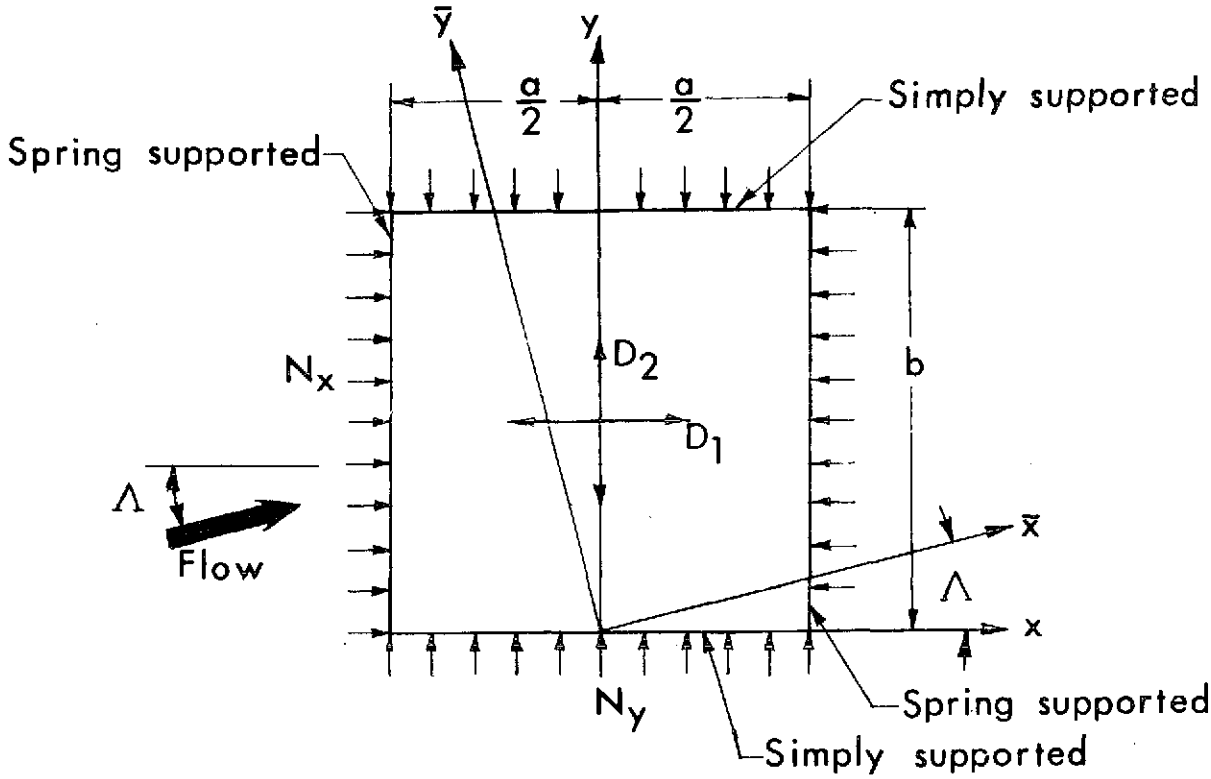

Figure 2.- Panel geometry and coordinate system.

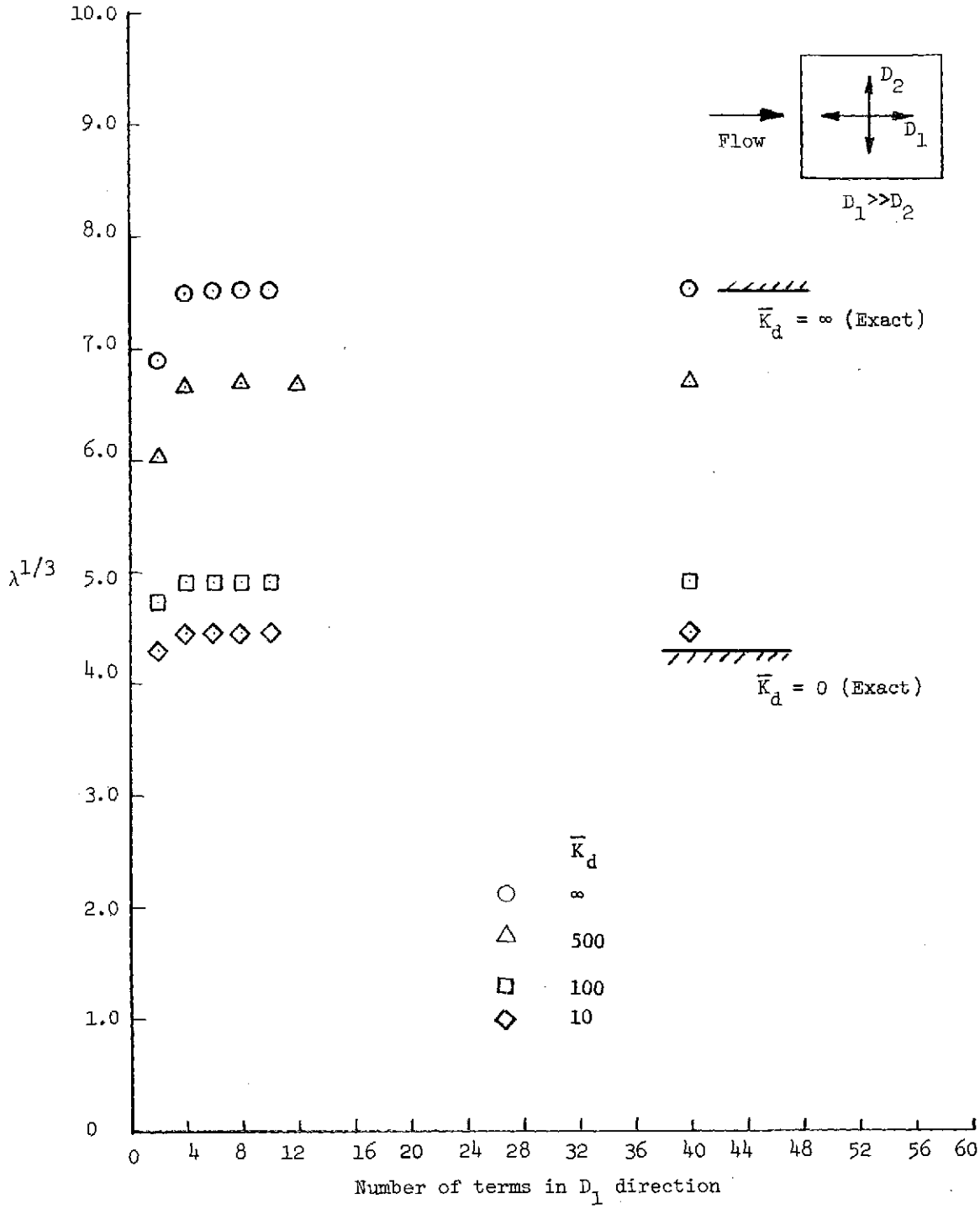

(a) $\Lambda = 0^{\circ}$, $n = 1$.

Figure 3.- Convergence of flutter data. $D_{12}/D_1 = 0.5$, $D_{12}/D_2 = 500$, $(a/b)^2 = 1.0$, $g_a = 0$, $g_b = 0$, and $g_m = 0$.

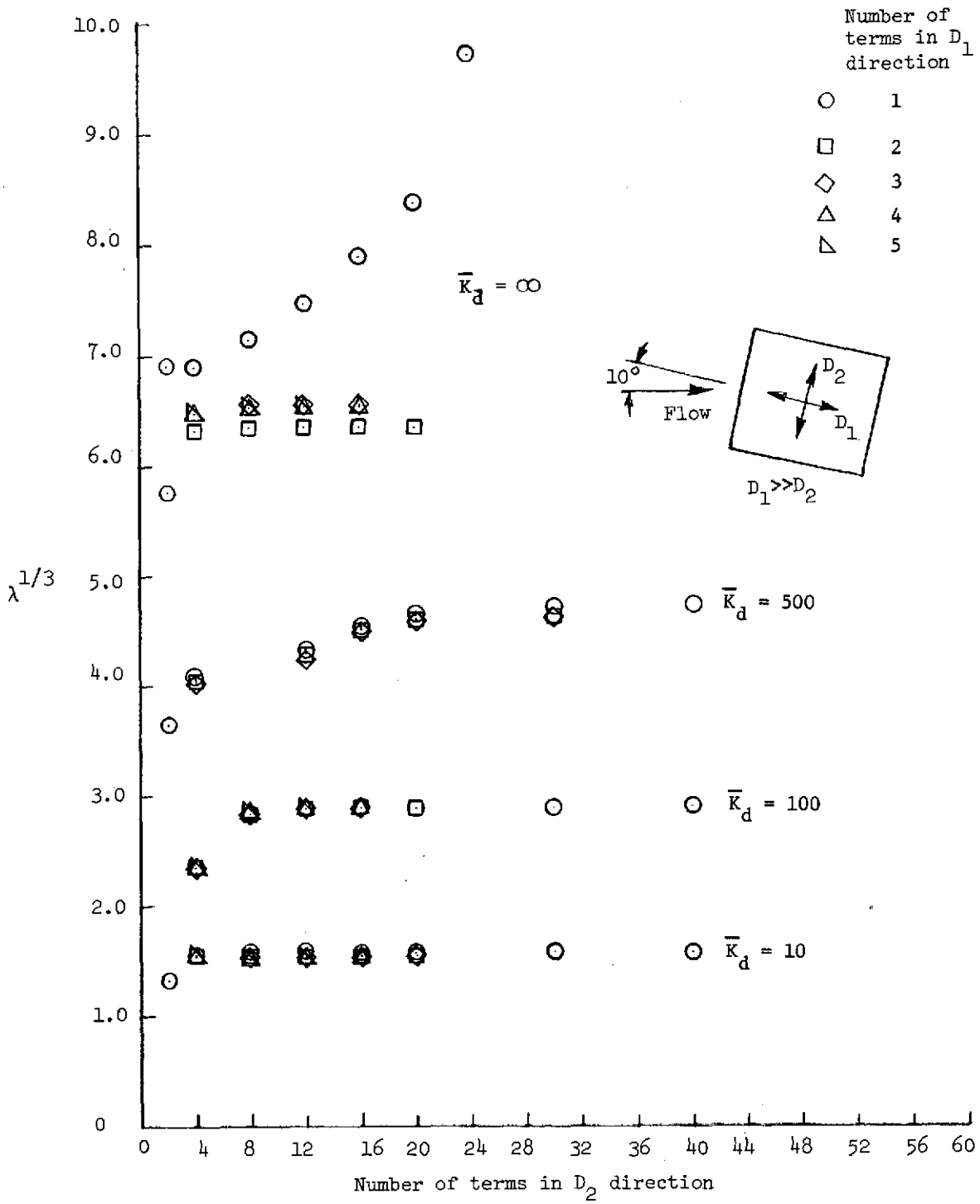

(c) $\Lambda = 10^{o}$.

Figure 3.- Concluded.

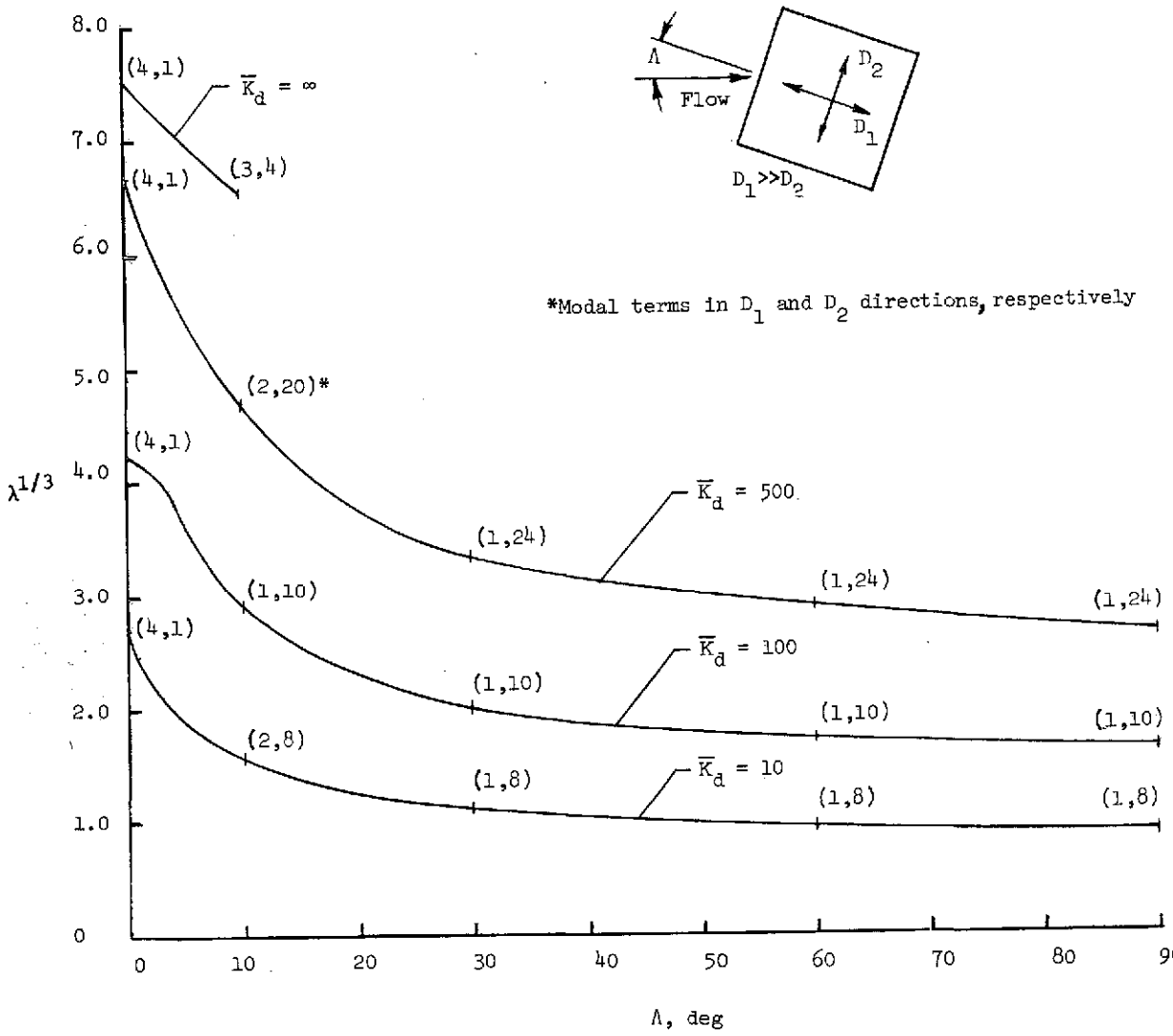

Figure 4.- Modal terms required for convergence as a function of cross-flow angle. $D_{12}/D_1 = 0.5$, $D_{12}/D_2 = 500$, $(a/b)^2 = 1.0$, $g_a = 0$, $g_b = 0$, and $g_m = 0$.

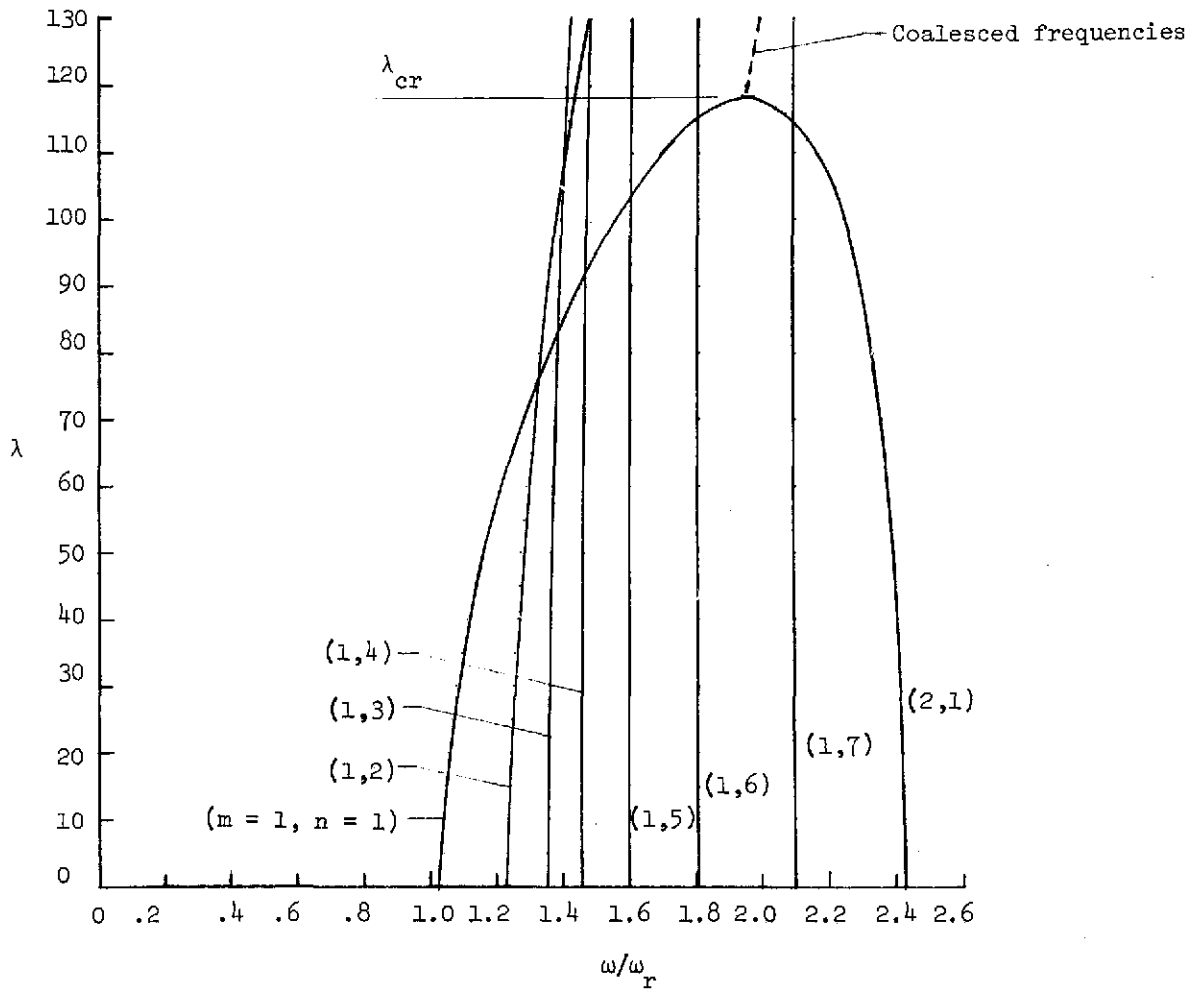

(a) $\Lambda = 0^{o}$.

Figure 5.- Variations of natural frequencies with dynamic-pressure parameter, λ. $D_{12}/D_1 = 0.5$, $D_{12}/D_2 = 500$, $(a/b)^2 = 1.0$, $\overline{K}_d = 100$, $g_a = 0$, $g_b = 0$, and $g_m = 0$.

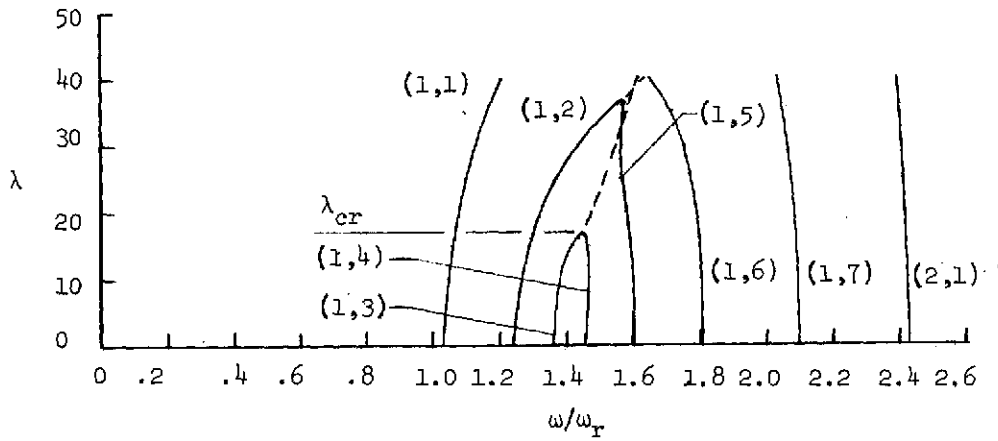

(c) $\Lambda = 15^{\circ}$.

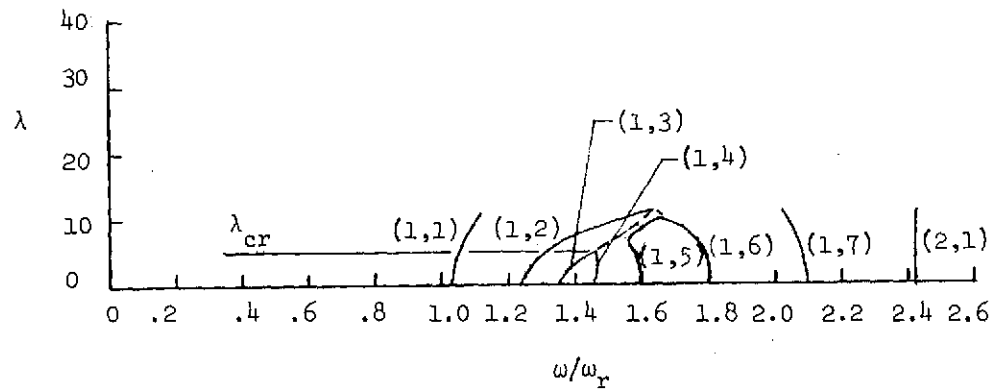

(d) $\Lambda = 90^{\circ}$.

Figure 5.- Concluded.

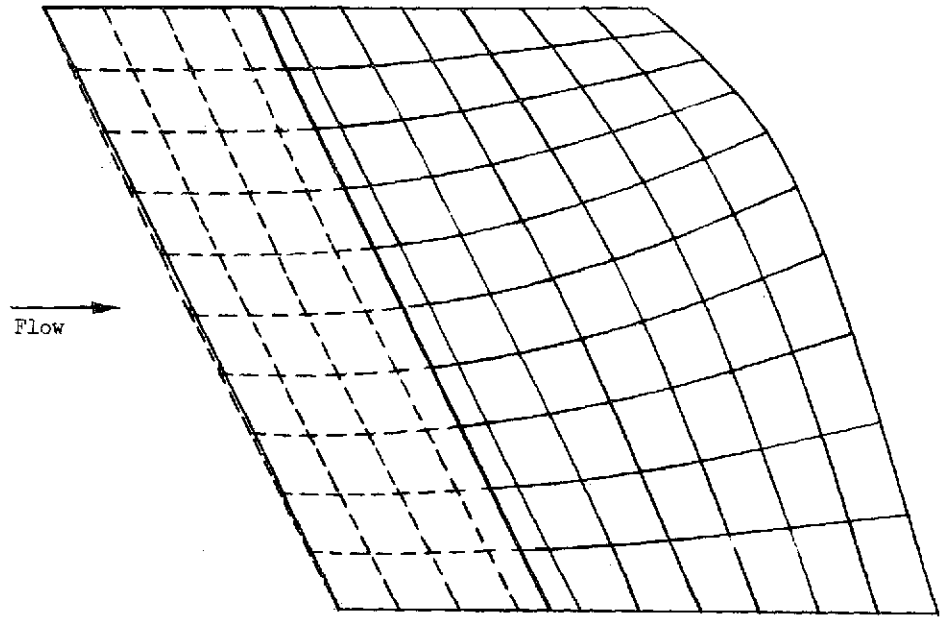

(a) $\Lambda = 0^{\circ}$.

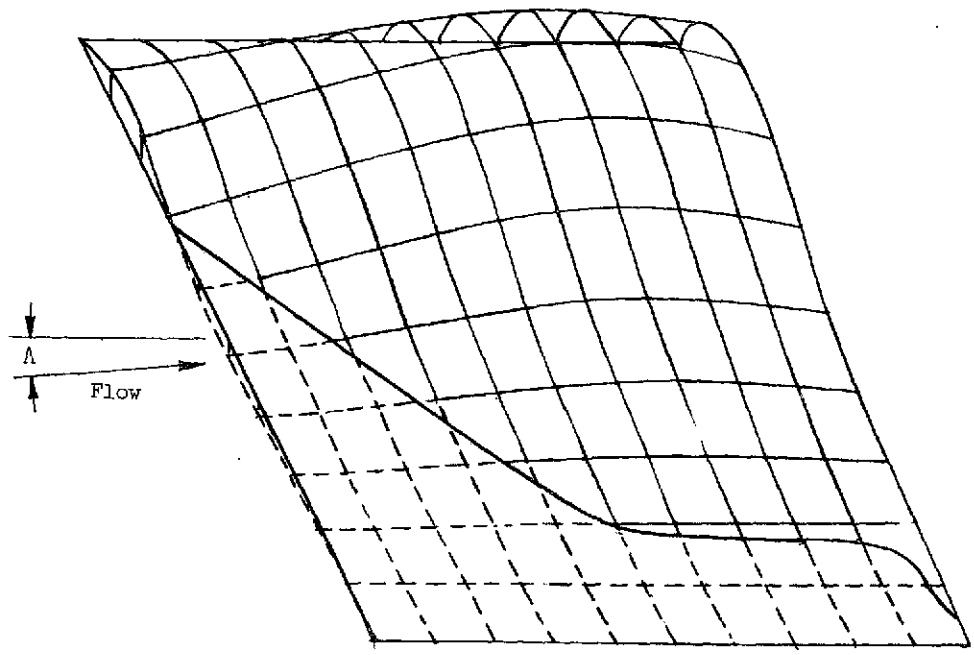

(b) $\Lambda = 2^{\circ}$.

Figure 6.- Theoretical flutter mode shapes. $D_{12}/D_1 = 0.5$, $D_{12}/D_2 = 500$, $(a/b)^2 = 1$, $\overline{K}_d = 100$, $g_a = 0$, $g_b = 0$, and $g_m = 0$.

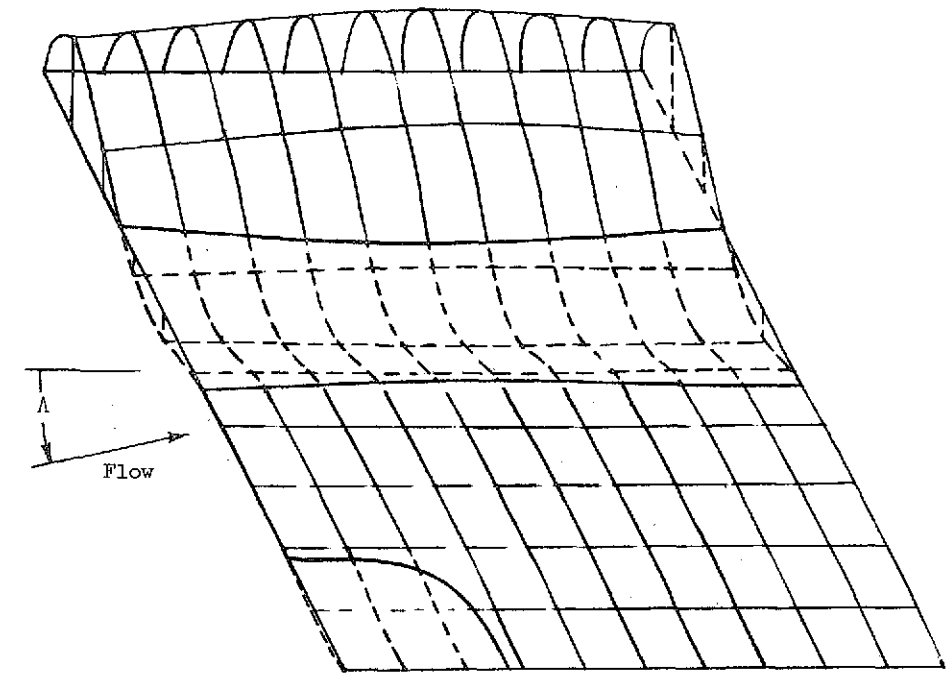

(c) $\Lambda = 15^{o}$.

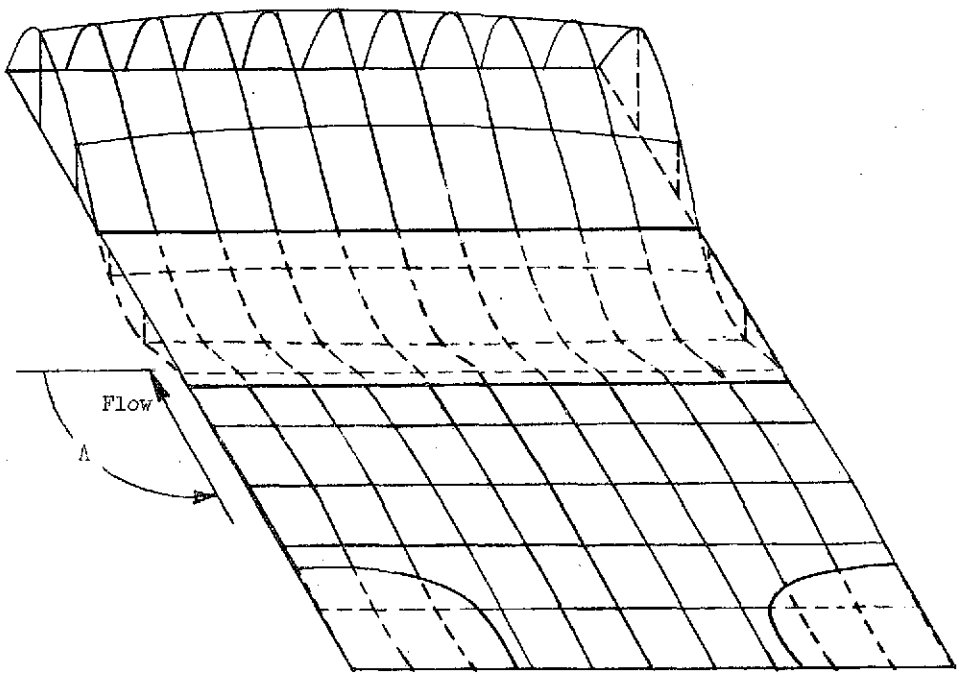

(d) $\Lambda = 90^{o}$.

Figure 6.- Concluded.

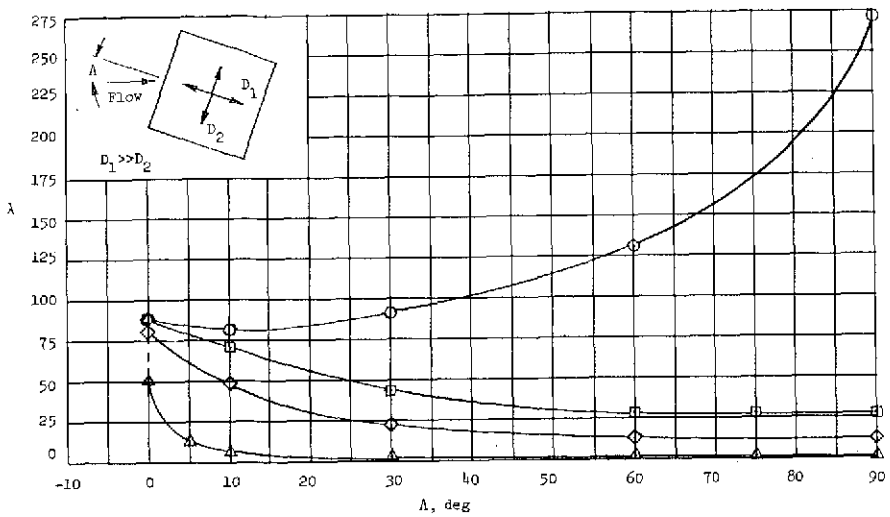

(a) $\overline{K}_d = 10.$

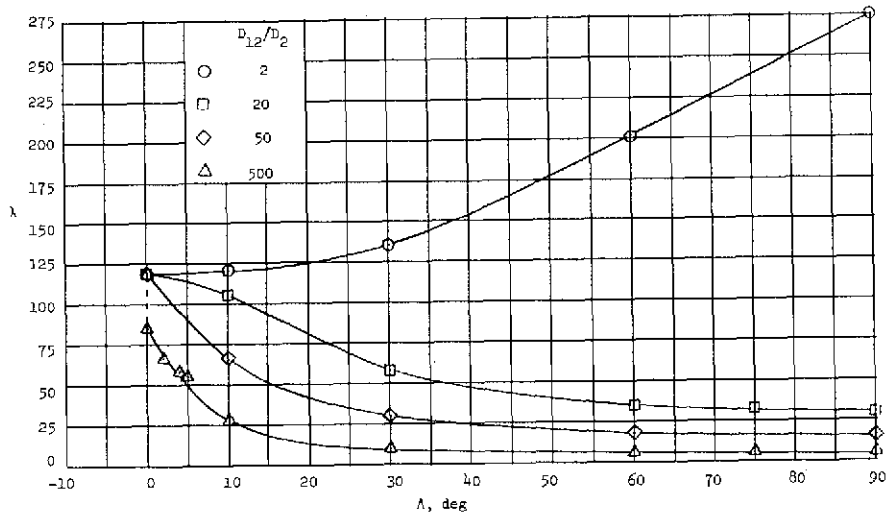

(b) $\overline{K}_d = 100.$

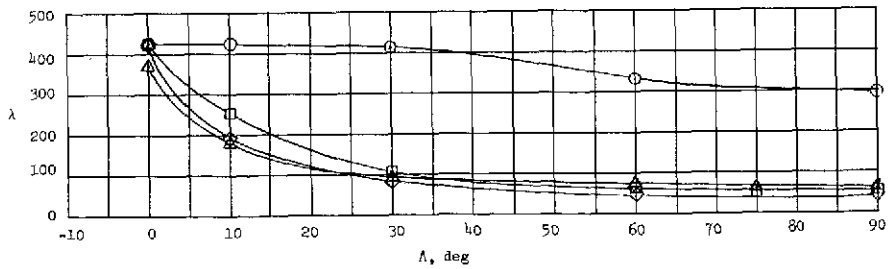

(c) $\overline{K}_d = \infty.$

Figure 7.- Effects of flow angle on flutter for $D_{12}/D_1 = 0.05$, $(a/b)^2 = 10$, $g_a = 0$, $g_b = 0$, and $g_m = 0$.

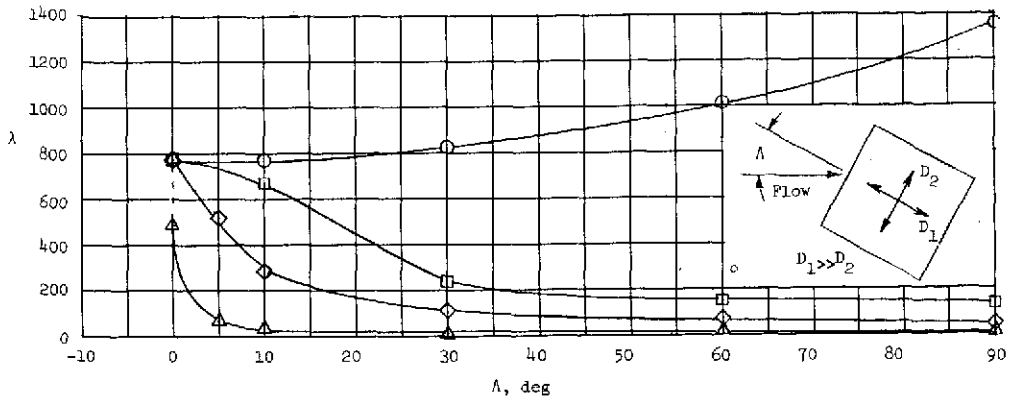

(a) $\bar{K}_d = 10.$

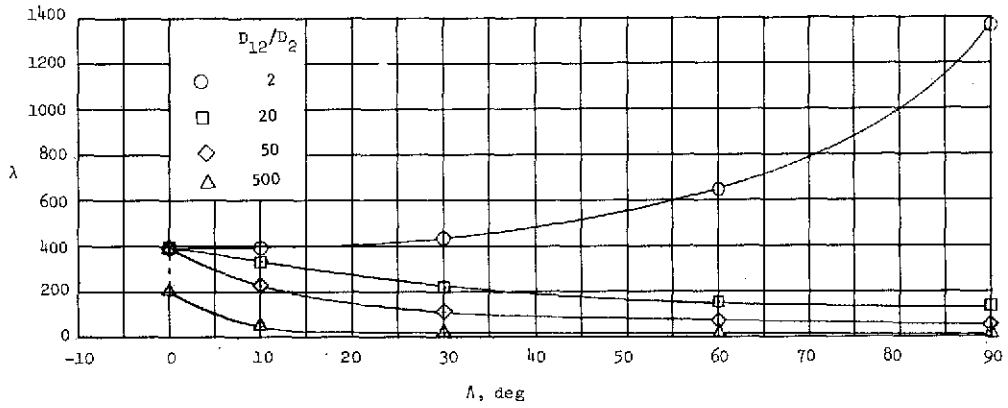

(b) $\bar{K}_d = 100.$

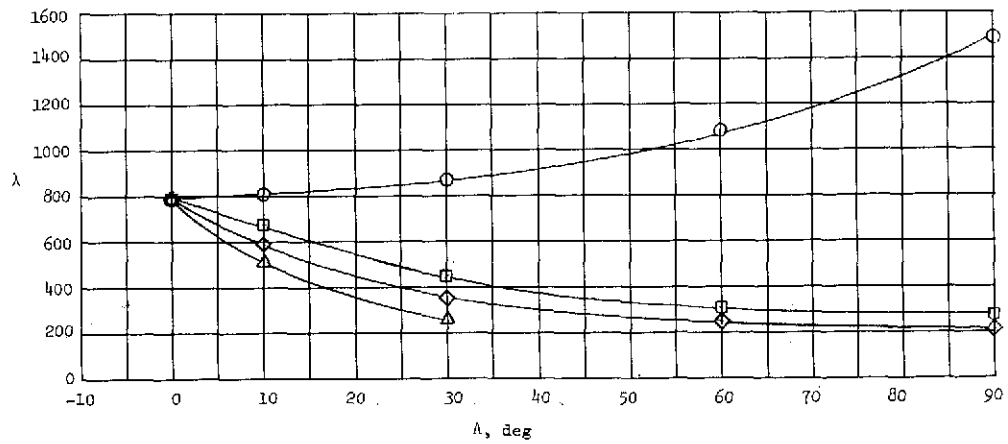

(c) $\bar{K}_d = \infty.$

Figure 8.- Effect of flow angle on flutter for $D_{12}/D_1 = 0.25$, $(a/b)^2 = 10$, $g_a = 0$, $g_b = 0$, and $g_m = 0$.

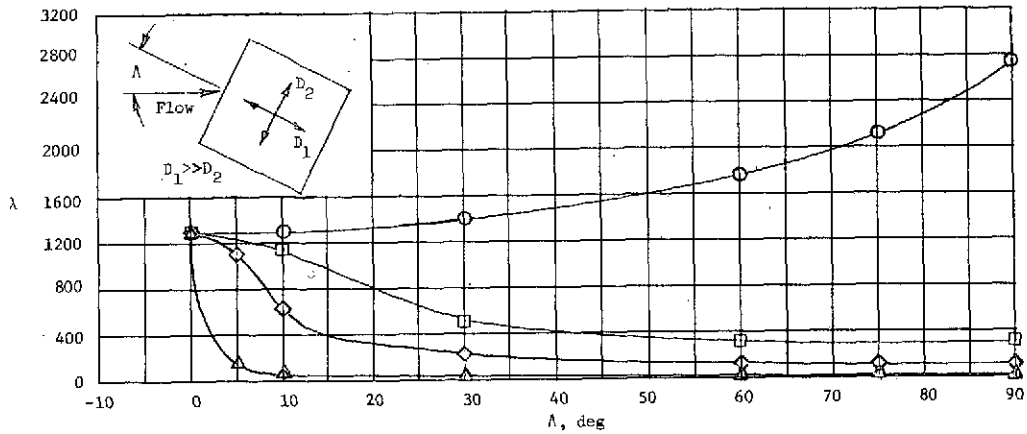

(a) $\overline{K}_d = 10.$

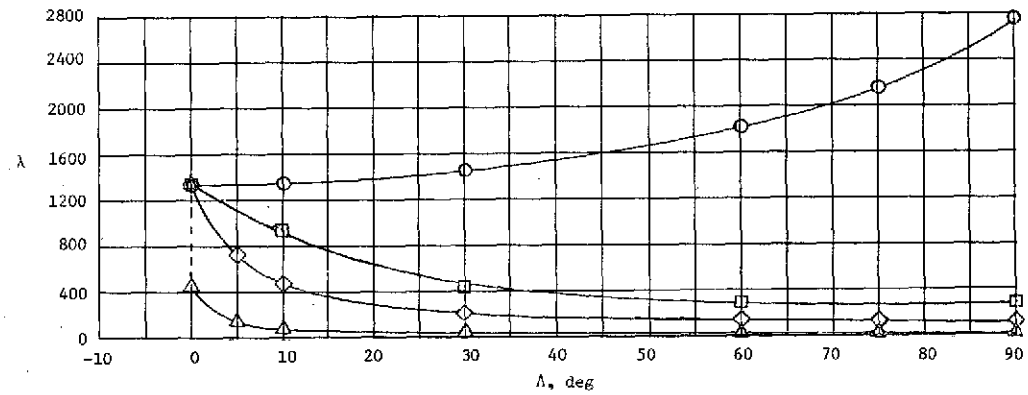

(b) $\overline{K}_d = 100.$

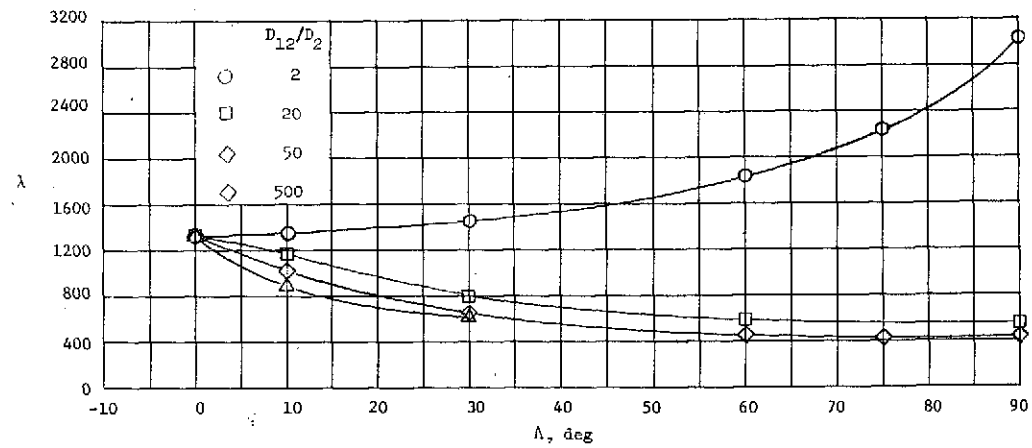

(c) $\overline{K}_d = \infty.$

Figure 9.- Effects of flow angle on flutter for $D_{12}/D_1 = 0.5$, $(a/b)^2 = 10$, $g_a = 0$, $g_b = 0$, and $g_m = 0$.

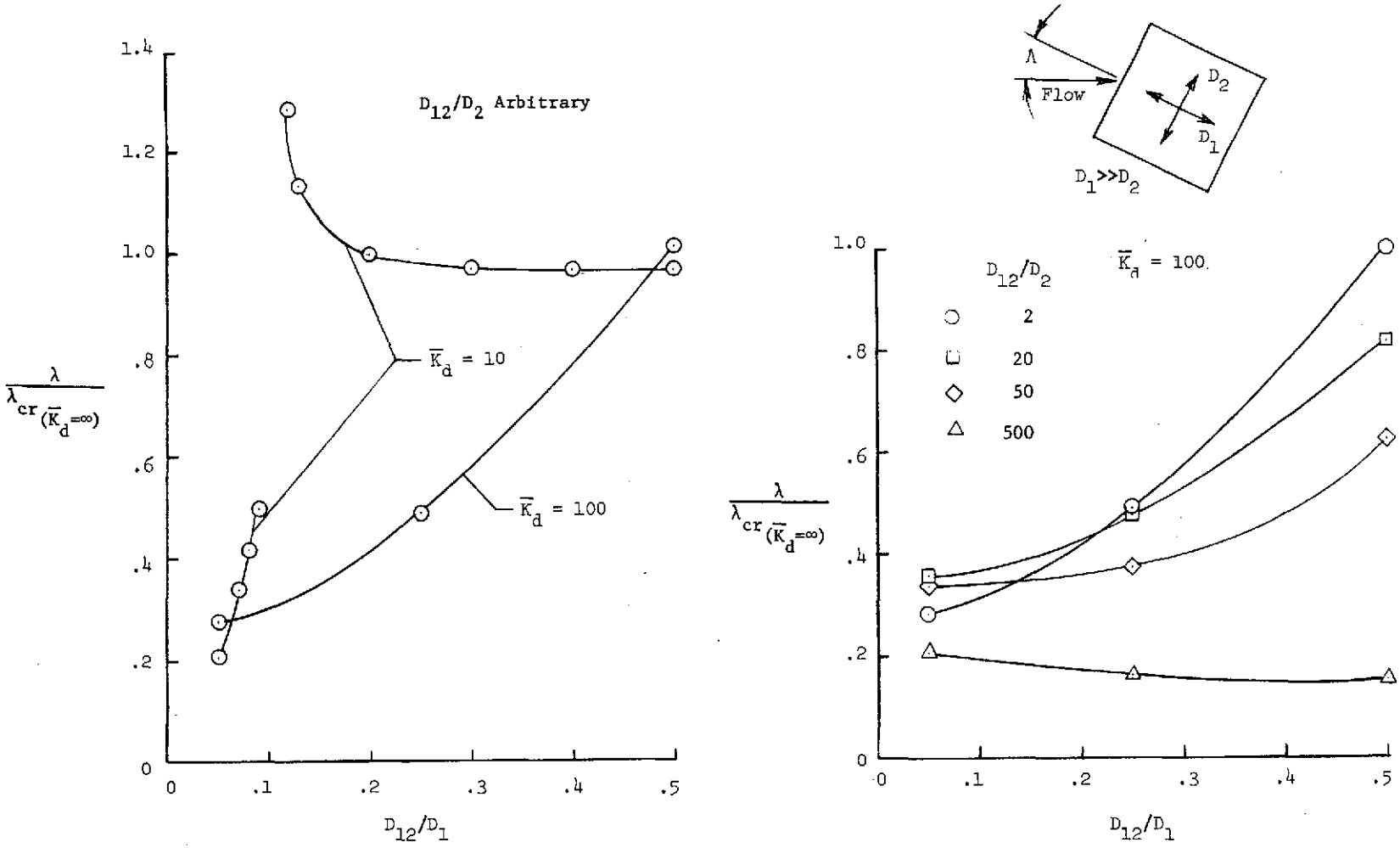

Figure 10.- Influence of panel flexural stiffness on flutter. $(a/b)^2 = 10$, $g_a = 0$, $g_b = 0$, and $g_m = 0$.

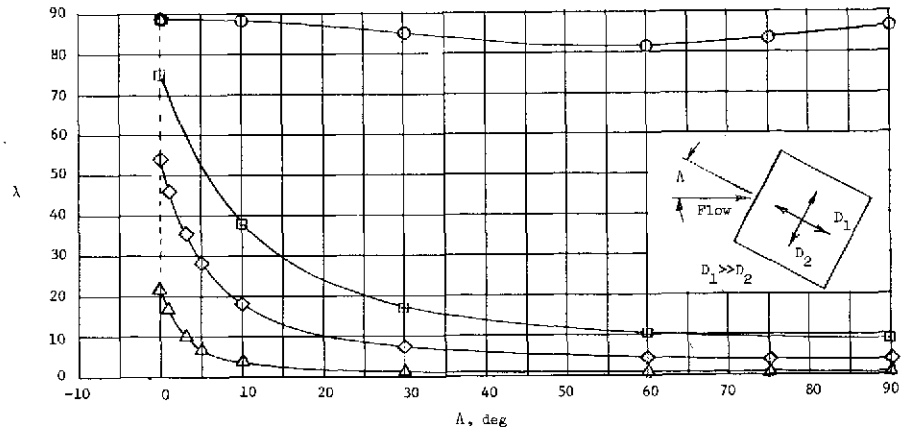

(a) $\bar{K}_d = 10.$

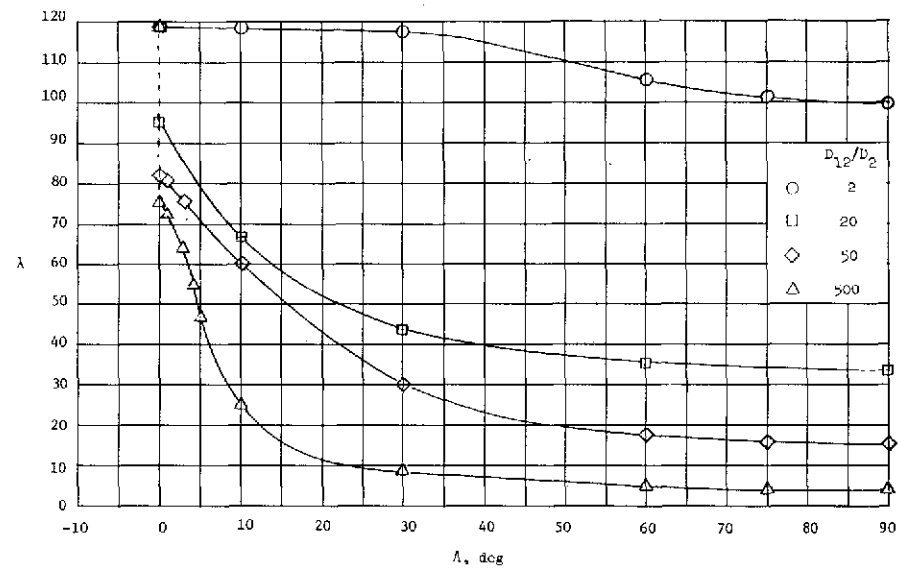

(b) $\bar{K}_d = 100.$

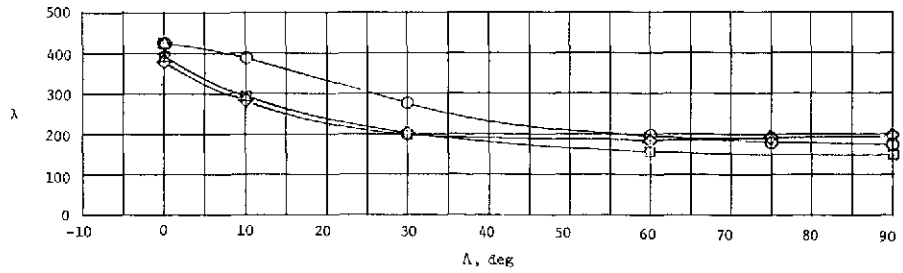

(c) $\bar{K}_d = \infty.$

Figure 11.- Effects of flow angle on flutter for $D_{12}/D_1 = 0.5$, $(a/b)^2 = 1.0$, $g_a = 0$, $g_b = 0$, and $g_m = 0$.

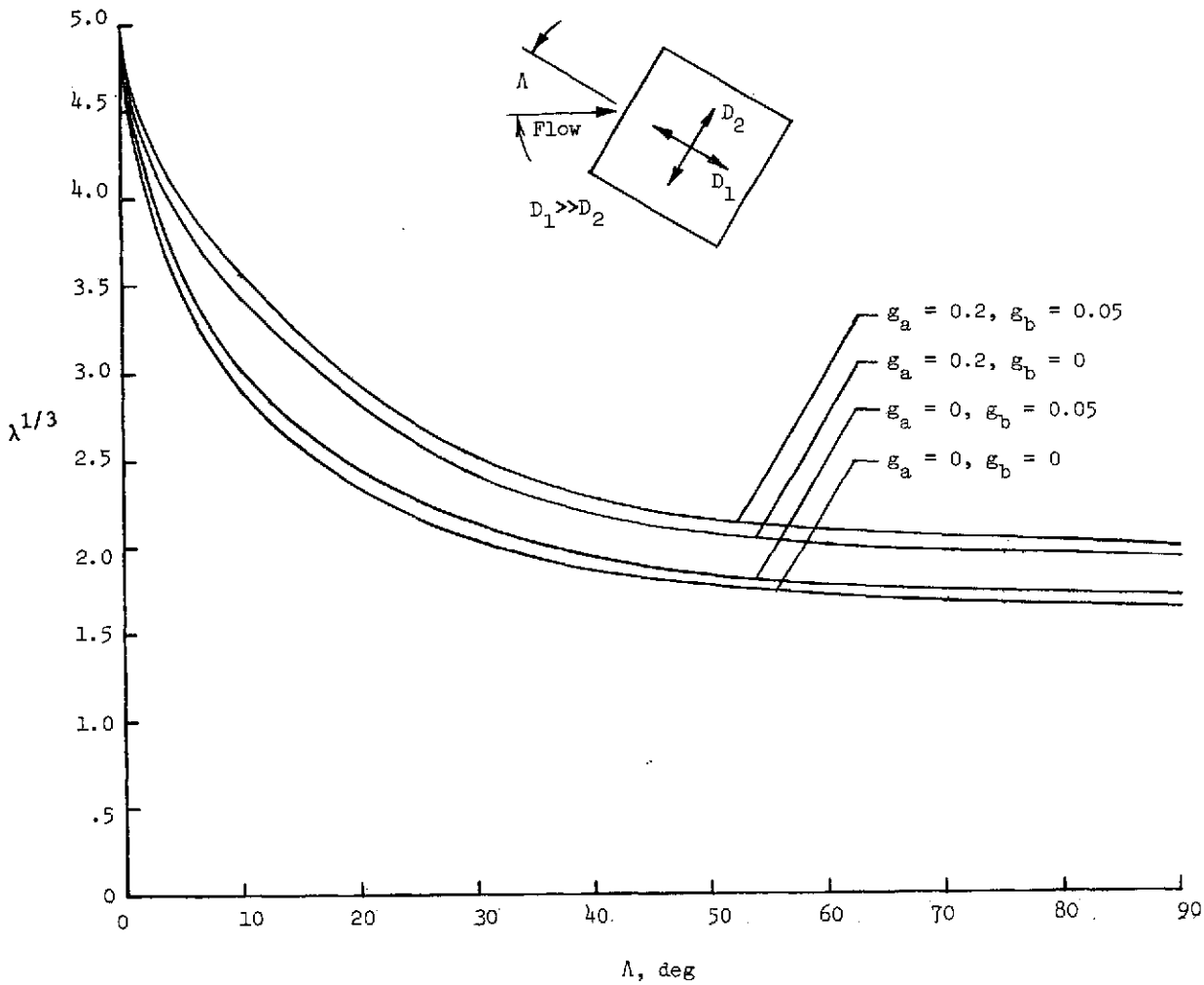

Figure 12.- Effects of aerodynamic and structural damping on flutter. $D_{12}/D_1 = 0.5$, $D_{12}/D_2 = 500$, $(a/b)^2 = 1.0$, $\bar{K}_d = 100$.

NASA-Langley, 1974 L-9312